King's Research Portal

Link to publication record in King's Research Portal

Dynamic field mapping and motion correction using interleaved double spin-echo diffusion MRI

Jana Hutter[1], Daan Christiaens[1], Maria Kuklisova-Murgasova[1],
Lucilio Cordero-Grande[1], Paddy Slator[2], Anthony Price[1], Mary Rutherford[1],
and Joseph V Hajnal[1]

Centre for the Developing Brain, King's College London, London, UK,
`jana.hutter@kcl.ac.uk`

Abstract. Diffusion MRI (dMRI) analysis requires the combination of data from many images and this generally requires corrections for image distortion, particularly in regions of varying susceptibility, and for subject motion during what may be a prolonged acquisition. The two can interact, and particularly in non-brain applications changes in pose such as through respiration can case the distortions to be time varying, so that correction with a static field map does not provide full correction. Also highly diffusion weighted (high b-value) images have low signal-to-noise ratio (SNR), which can make motion estimation using image registration problematic. In this work we develop an approach that breaks the traditional "one-volume - one-weighting" paradigm by interleaving low- and high-b slices in every volume and we combine this with a phase-encoding reversed double-spin echo sequence. Interspersing low and high b-value slices within each acquired volume, ensures that there is always higher SNR, low b, data in close spatial and temporal proximity to support field map determination from the double spin echo and motion estimation based on image registration. This information can be propagated to low SNR, high b, slices by local interpolation across space and time. The method is tested in the challenging environment of fetal dMRI and it is demonstrated using data from 8 pregnant volunteers that combining dynamic distortion correction with slice-by-slice motion correction increases data consistency to produce data suitable for advanced analyses where conventional methods fail.

1   Introduction

The unique ability of diffusion MRI (dMRI) to probe microstructural complexity with advanced biophysical modelling techniques facilitates detecting local tissue changes and estimating global connectivity patterns in the brain [6]. Emerging applications such as fetal dMRI may lead to new insights in human brain development, but are complicated by subject motion and image distortion.

Fetal imaging is prone to motion artifacts due to maternal breathing and the fetal movement itself. While frequently employed 2D single shot echo-planar imaging (ssEPI) is quick enough to freeze intra-slice motion, it does not resolve

inter-slice motion, so that the stacks of slices needed to capture whole volumes typically feature inconsistent and highly variable slice locations. Existing techniques reconstruct a motion-corrected volume from these scattered slices using slice-to-volume registration [9]. However, this is challenging at high b-values because the strong signal attenuation and the absence of consistent anatomical features makes these images poorly suited for standard image registration [3].

Geometric image distortion due to magnetic field susceptibility is particularly prominent in EPI imaging due to the low read-out bandwidth. Traditional distortion correction often uses static field maps, either acquired separately or calculated in post-processing from an image pair with reversed phase encoding directions [1]. Furthermore, in fetal applications, changes of the maternal pose due to respiration, as well as the proximity of gas in the maternal bowel can result in *time-varying* susceptibility induced distortions. Traditional techniques that assume static single time point field maps are unhelpful in this scenario, and the move from 1.5T to 3T for advanced fetal studies has exacerbated these problems, particularly with long scan durations needed for eloquent dMRI data.

In this work, we develop an integrated novel acquisition and pre-processing strategy which tries to address these challenges by breaking the fundamental traditional acquisition paradigm of "one volume, one diffusion gradient (b-value and direction)". While conventional dMRI sequentially acquires all slices per volume with a given diffusion weighting, our method interleaves slices with low and high b-values within each slice stack. In addition, acquisition of a second spin-echo with reversed phase encoding at each ssEPI shot provides data usable for distortion correction for each individual slice [5]. The combination of these elements ensures that there can be low-b information suitable for distortion and motion correction obtained at high temporal resolution, while all required b-values can be obtained for all slices within a super cycle.

2 Methods

2.1 Acquisition I: Interleaved diffusion MRI

The acquisition yields a sequence of image intensity vectors $\boldsymbol{y}_t$ per slice at time stamps $t \in [1, \ldots, N_d \cdot N_s]$, where N_d specifies the number of diffusion gradients and N_s the number of slices per volume. Each observation $\boldsymbol{y}_t$ is thus described by a geometric index s, a diffusion index d (associated with a b-value (bval) and sensitization direction (bvec)), and its time stamp t.

While in conventional dMRI the N_s slices acquired during each repetition time period, TR, share the same diffusion index d (see Fig. 1a), our technique breaks this continuity (Fig. 1b) and thus reduces the time between sequential low-b data points. An ideal design maximally interleaves low and high b-values for these two goals, but ensures that as many complete volumes of constant b data are obtained even as possible even if the scan is interrupted or abandoned. Therefore, a super cycle bloc design with length N_i is chosen ($N_i = 5$ in Fig. 1b), where N_i consecutive b-value samplings are interleaved so that all slices are
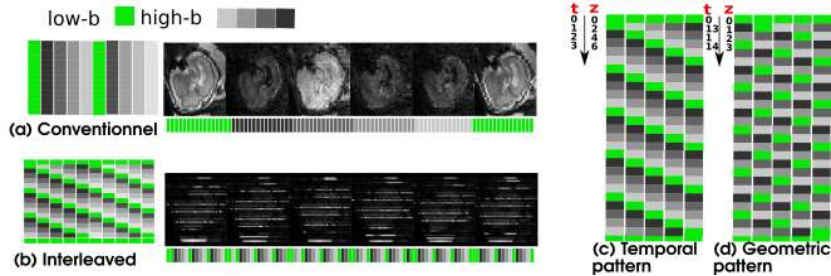
Fig. 1: The schematic diffusion volume vs. slice representation (*b*-value in color: low-*b* in green, high-*b* values in grey.). (a) The traditional one volume, one diffusion gradient sampling approach, and the resulting data reformatted so that the slice direction is along the vertical axis; (b) The proposed sampling with interleaved diffusion sampling for all slices and its corresponding reformatted data. Six consecutive volumes as acquired are shown in both cases. (c,d) For a given acquisition order of 0-2-4-6 ... 1-3-5-7 ... the (c) temporal sequence of weightings and the corresponding (d) spatial sequence of weightings is shown.

acquired with all diffusion weightings (i.e. *b*-value shells) after N_i volumes. The number of required blocks depends on the total number of diffusion samples.

Furthermore, the spatial *z*-location of the slices constitutes a second dimension to be considered. To ensure optimal registration properties, the low *b*-value data was not only spread out maximally in time, to densely sample motion patterns, but also in space to ensure spatial proximity of every high-*b* slice to a low-*b* slice. This was achieved by maximizing the inter-slice to inter-shot distances. For example, for the frequently used even-odd slice ordering (0-2-4-6.1-3-5-7), this requires that low-*b* slices are acquired every N_i shots such that the step stride wraps between slice groups. See Fig. 1c and d for an example with $N_s = 25$, $N_i = 5$. To further facilitate registration, the top and bottom slice of every volume is acquired with $b = 0$ (see Figure 1b). In addition to the main dMRI data set, three additional volumes consisting only of $b=0$ slices may be acquired in an orthogonal imaging plane to further help volumetric recovery.

2.2   Acquisition II: Double spin-echo

The EPI sequence features a double spin echo, with the second echo obtained with opposed phase encoding direction (see Fig. 2). While differing in echo time and thus contrast and signal, the two echoes have matched read-out bandwidth but opposite susceptibility induced shift effects/distortions. Their temporal proximity of < 100 ms and the need for a coherent signal pathway throughout the sequence to obtain signals, ensures that the two images produced per slice can be relied up on to have closely matched (nominally identical) motion states. Susceptibility induced stretching in the first echo (Fig. 2 yellow) corresponds to signal pile-up in the second echo (red). This novel capability, including all required modifications (gradient duty cycle, reconstruction and slice ordering) was implemented on a Philips 3T-Achieva scanner (R3.2 software).
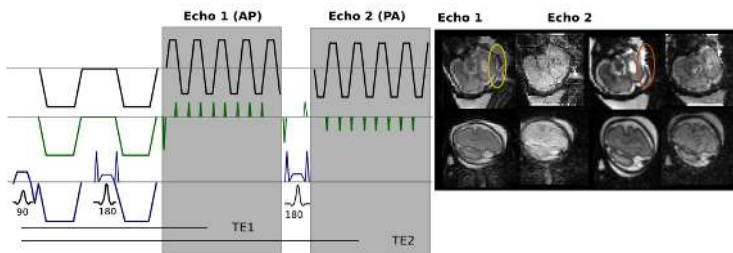
Fig. 2: (a) Sequence diagram (simplified) of the double spin-echo sequence. (b) Acquired echoes with opposed phase encoding and thus equal-opposite distortions.
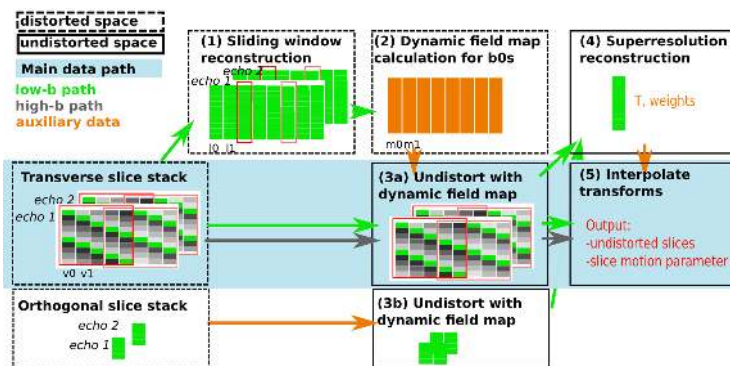

Fig. 3: Illustration of the processing algorithm from the acquired interleaved stacks (left) to the final distortion and motion-corrected dMRI volumes (right). The steps include (1) sliding window volume assembly, (2) dynamic field map calculation, (3) undistortion, (4) superresolution reconstruction and motion correction for low-b slices and (5) propagation of corrections to rest of slice data.

2.3 Post-processing algorithm

The acquired interleaved double spin-echo data point pairs $\boldsymbol{y}_t^{\{AP,PA\}}$ represent individual samples, differing by geometric location and diffusion weighting. They form the data input for a bespoke 5 step post-processing framework developed in-house using IRTK building on [10, 7], as illustrated in Fig. 3.

Dynamic distortion correction The acquired double-spin echo interleaved diffusion data is first re-ordered to assemble low b-value volumes using a sliding window approach (step 1). Each temporal volume T_v gathers together the temporally closest low-b slices. The window size equals the interdiff factor, N_i, and the maximal temporal distance to measured distortion correction data thus equals 2TR for the case of $N_i = 5$ illustrated. This data is used (step 3) to calculate fieldmaps (in Hz) for every time point using FSL `topup` [1].

In step 3, the temporally closest fieldmap is chosen to correct each slice for distortions. This operation is performed in scanner coordinates and the field maps are converted into displacements in mm taking the bandwidth of the sequence and the EPI factor into account.

Motion correction In step 4, all the low-b volumes as well as the two or three additionally acquired orthogonal low-b volumes are combined as input to a slice-to-volume (SVR) alignment and reconstruction process [7] to create a geometrically self consistent 3D fetal brain volume. The process intersperses a registration step to progressively refine the position estimate of each slice in anatomical space, with a super-resolution reconstruction step that uses all newly aligned data to generate a 3D volume that can then be used as a registration target for the next iteration. To aid convergence, initially each complete low-b volume is registered to the mean of all other low-b volumes, then all slices in the low-b volume are resorted into groups depending on their acquisition time (spread over N_i TRs) and registered in these groups to the volume, and finally every individual slice is registered. This allows the position of each slice to be refined while accounting for temporal proximity. The outcome of this processing step is a super-resolved low-b volume, transformation parameters $(t_x,t_y,t_z,r_x,r_y,r_z)$ for each individual low-b slice, and a weight assigned to each slice according to how consistent its signals are compared to the co-located data from other aligned slices. The latter information is useful for outlier rejection.

Full data correction In step 5, all the remaining higher b-value slices are distortion corrected using the temporally closest field map and individually assigned a positional transformation obtained by interpolation of the transformations for the two closest low-b slices in time. The result of this step is a set of geometrically precise slices with the transformations that project them into a self consistent anatomical space—prepared for any post-processing method which can deal with a scattered data space. Direct estimation of derived parameters such as for example the spherical harmonic (SH) coefficients is possible [8].

2.4   Experiments

To illustrate the technique, 8 pregnant volunteers (gestational age 26-34 weeks) were studied using a 32-channel cardiac coil and the proposed double spin-echo interdiff sequence to acquire 3-shell HARDI data with a total of 49 directions (11 $b = 0$, 8 $b = 400$, 30 $b = 1000$ s/mm²), isotropic resolution 2.2 mm³, 34-36 slices/volume, $N_i = 5$, TR 11000 s-15000 s, TE 107 ms for the first echo and 208 ms for the second echo, SENSE 2.0, using image-based shimming and fat suppression. In addition, on 4 of these volunteers, sagittal double spin-echo dMRI data with 3 $b0$ volumes was acquired with similar imaging parameters.

3   Results

3.1   Dynamic field mapping and motion correction

The dynamic calculation of a field map based on sparse but frequently acquired $b0$ slices provides significant improvement in the presence of motion or varying B0-fields (e.g. as a result of intestinal gas bubbles). To assess the goodness of

(a) Correlation AP/PA (mean)

(b) Correlation AP/PA over time volumes e

(c) Fieldmap for subject 8

(d) Correction results (subject 8)

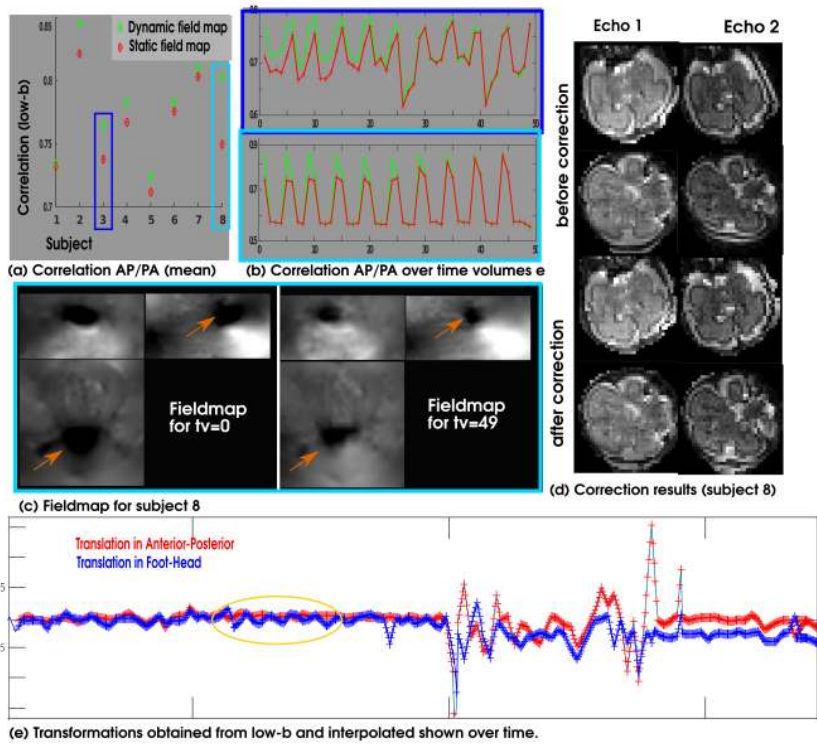(e) Transformations obtained from low-b and interpolated shown over time.

Fig. 4: Results from distortion correction using the dynamic maps. (a) Mean over the correlations between AP/PA images for all low-b volumes are shown for the dynamic field map (green) vs. the static fieldmap acquired at the acquisition end (red). (b) The correlation for every diffusion weighting is shown for both corrections for subject 3 and 8. (c) Fieldmaps from the acquisition start and end and (d) correction results are shown for subject 8. (e) Translation parameters are shown for anterior-posterior and foot-head direction.

the distortion correction based on these maps, the data from both echoes was distortion corrected twice: (i) with the obtained dynamic fieldmap using the described acquisition and processing steps, and (ii) using a static fieldmap obtained from a non-interleaved acquired double spin-echo pair at the end of the acquisition. The data from both phase encoding directions was then vectorized and their correlation coefficient per diffusion direction calculated. The time series of mean correlations for the low-b volumes is shown in Fig. 4a. The correlation per volume for static (red) and dynamic (green) distortion correction in (b) shows that dynamic field mapping achieves consistently high correlations. The short term oscillations reflect intrinsic variation in correlation caused by the different SNR of low and higher b-value data. Static distortion correction improves towards the end of the series, which is when the static field map was acquired. The upper panel illustrates a case with extensive fetal motion, illustrating improved correction for all volumes in the proposed approach. The lower panel illustrates a case where fetal motion is limited but the fieldmap changes over time due to
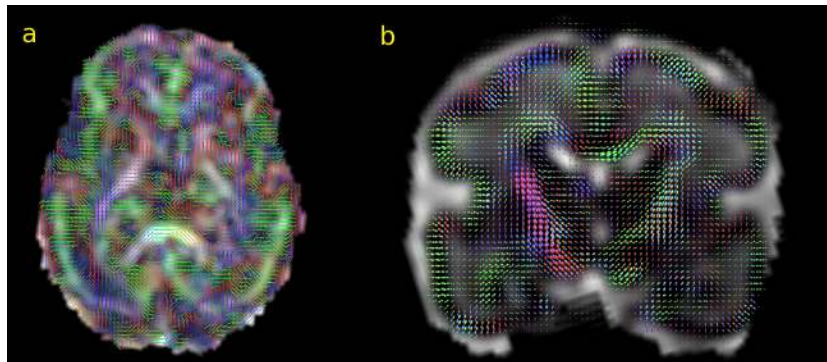
Fig. 5: (a) Axial slice of the fractional anisotropy (FA) map after dynamic distortion and motion correction, overlaid with the principal eigenvectors of the diffusion tensor fit. (b) Coronal slice of a multi-shell multi-tissue decomposition of the same reconstructed data. Vectors and ODFs are coloured according to their direction in the scanner coordinate system, not the subject space.

maternal bowel gas movement, as shown in (c) at the start and end of the sequence. Here, the proposed method significantly improved the consistency of the low-b volumes. Finally, the data from both echoes is shown before and after correction in (d), indicating high degree of geometrical consistency that is achieved between the echoes (a sign of precise distortion correction). The proposed correction framework was successful in all the subjects studied. The SVR algorithm (step4-5) using all low-b slices provided robust motion estimations (Fig. 4e) depicting the breathing cycle of the mother (orange ellipse) in periods of limited fetal motion.

3.2 Derived quantitative dMRI information

The final dynamic distortion and motion corrected data is suitable for advanced dMRI analysis, including tractography and microstructural modelling. Here, we assess the overall quality of the data using conventional diffusion tensor imaging (DTI) [2] and using a multi-shell spherical factorization [4] with two tissue components for brain tissue (SH order 4) and free water (isotropic). Figure 5 shows fractional anisotropy (FA) images, principal DTI eigenvectors, and tissue orientation distribution functions (ODFs) of a single fetus. These results show high anisotropy in the cortex and maturing white matter structures such as the splenium, as expected in early brain development. The eigenvectors and ODFs are well aligned with developing white matter structures and with cell development perpendicular to the cortical surface. These results illustrate the practical applicability of our method in clinical assessment.

4 Discussion and conclusion

We presented a method for acquiring and processing dMRI data that is designed to facilitate both distortion and motion correction. The approach allows

dynamic distortion correction with a data derived field map generated every N_i TRs, which for the examples shown means the closest distortion estimate is only 2TR, or 22-30 sec, distant. Motion correction estimates interpolate between low-b slices that are $(N_i/N_s)\cdot$ TR apart, which for the examples shown is around 1.6 sec. Inclusion of sufficient low-b slices poses an additional constraint to the optimal sampling scheme, but can include a range of b-values dispersed across lower shell(s) and thus add to the analysis. The choice of the threshold between low b-value (used for active distortion and motion correction) and high-b value (which are to be corrected) depends largely on the obtained SNR. In the pilot testing done so far the approach proved robust and effective, with clear evidence of both distortion and motion correction found in each subject. The full interleaving of high and low b-value slices can also offer benefits in reducing gradient demand, hence allowing more efficient scanning. Future work could include advanced transformation interpolation techniques as well as outlier detection algorithms. The fully flexible framework presented proved effective in the fetal dMRI application tested, but clearly is widely generalizable to any diffusion study that includes high b-values. Our full post-processing pipeline will be made publicly available.

References

1. Andersson J and Skare S: A model-based method for retrospective correction of geometric distortions in diffusion-weighted EPI. NeuroImage 16, 177-199 (2002)
2. Basser PJ, Mattiello J, LeBihan D: MR diffusion tensor spectroscopy and imaging. Biophysical journal 66(1), 259-267 (1994)
3. Ben-Amitay S, Jones DK, Assaf Y: Motion correction and registration of high b-value diffusion weighted images. Magn. Reson. Med. 67(6), 1694-702 (2012)
4. Christiaens D, Sunaert S, Suetens P, Maes F: Convexity-constrained and nonnegativity-constrained spherical factorization in diffusion-weighted imaging. NeuroImage 146, 507-517 (2017)
5. Gallichan D, Andersson J, Jenkinson M, Matthew D, Robson M, Miller K: Reducing Distortions in Diffusion-Weighted Echo Planar Imaging With a Dual-Echo Blip-Reversed Sequence. Magn. Reson. Med. 64, 382-390 (2010)
6. Jones DK: Diffusion MRI: Theory, Methods and Applications. Oxford University Press (2010)
7. Kuklisova-Murgasova M, Quaghebeur G, Rutherford MA, Hajnal JV, Schnabel JA: Reconstruction of fetal brain MRI with intensity matching and complete outlier removal. Medical Image Analysis 16(8),1550-64 (2012)
8. Kuklisova-Murgasova M, Rutherford MA, Hajnal JV: ISMRM 2017, p. 4484
9. Oubel E, Koob M, Studholme C, Dietemann J-L, Rousseau F: Reconstruction of scattered data in fetal diffusion MRI. Medical Image Analysis 16(1):28-37 (2012)

10. Rueckert D, Sonoda L, Hayes C, Hill D, Leach MO, Hawkes DJ: Non-rigid registration using free-form deformations: Application to breast MR images. IEEE Transactions on Medical Imaging, 18(8), 712-721 (1999)